PERGAMON

International Journal of Solids and Structures 36 (1999) 345–361

INTERNATIONAL JOURNAL OF SOLIDS and STRUCTURES

Saint-Venant's principle and the plane elastic wedge

N. G. Stephen*, P. J. Wang†

Department of Mechanical Engineering, The University of Southampton, Southampton, SO17 1BJ, U.K.

Received 4 June 1996; in revised form 7 January 1998

Abstract

The stress field due to self-equilibrating loading on the inner or outer arc of a plane strain elastic wedge sector is affected by two agencies: a geometric effect of increasing or decreasing area, and decay as anticipated by Saint-Venant's principle (SVP). When the load is applied to the inner arc the two effects act in concert; however, when the load is applied to the outer arc the two effects act in opposition and for a wedge angle in excess of the half-space, $2\alpha > \pi$, for the symmetric case, and for $2\alpha > 1.43\pi$ for the asymmetric case, the geometric effect is dominant over Saint-Venant decay and stress level increases as one moves away from the outer arc, confirming the inapplicability of SVP. This is additional to previously reported difficulties at these angle when a self-equilibrated load on the inner arc decays at the same rate as does a concentrated moment, and is explained in terms of the interaction of a near-field geometric effect and a far-field stress interference effect at a traction-free edge. For wedge angle $2\alpha = 2\pi$ the unique Modes I and II inverse square root stress singularities at the crack tip, which are at the heart of Linear Elastic Fracture Mechanics (LEFM), can be attributed to this inapplicability for just one symmetric and one asymmetric eigenmode.

1. Introduction

The classical Carothers (1912) solution for a wedge subjected to a concentrated moment at the apex shows pathological behaviour at the critical wedge angle $2\alpha = 2\alpha^* \approx 1.43\pi \approx 257^\circ$; this well known paradox has been investigated by many researchers (see Dundurs and Markenscoff (1989) for a review of the literature). In a recent paper, Markenscoff (1994) attributes this breakdown in the solution to a failure of Saint-Venant's principle (SVP), and describes three methods of applying the concentrated moment, these being

(a) the original Carothers solution in which the truncated wedge experiences a moment on the inner arc r_i and then allowing $r_i \to 0$.

* Author to whom correspondence should be addressed. Fax: 441703593230. E-mail: ngs@soton.ac.uk.

† Visiting Professor from Department of Mechanical Engineering, Shanghai Maritime Institute, Shanghai, 200135, P.R. China.

0020–7683/99/$ - see front matter
PII: S0020–7683(98)00026–2

(b) a first alternative, due to Sternberg and Koiter (1958), in which the moment is applied on the flank of the wedge over some length a, and then setting $a \to 0$.
(c) a second alternative, originally due to Neuber (1963), in which the moment is applied by means of a twisted plug of vanishing radius applied at an interior point approaching the apex.

All three cases have the same far-field solution for wedge angles smaller than the half-space, that is $2\alpha < \pi$; this is as it should be if SVP applies. For the half-space and at the critical wedge angle $2\alpha^*$, SVP is known to be inapplicable in the sense that symmetric and asymmetric self-equilibrating loads, respectively, can decay at the same rate as does a concentrated moment applied at the apex, the latter due to diffusion of stress into a divergent cross-sectional area. As indicated by Sternberg and Koiter (1958), while this may not be in conflict with a rigorous statement of the principle, it is in striking contradiction to a conventional interpretation of SVP. As will be seen, further difficulties in the application of SVP are evident when one considers self-equilibrated loading on the outer arc.

Consider an incomplete elastic ring with loading applied to the inner and outer arcs $r = a$, $r = b$, respectively, while the flanks $\theta = \pm\alpha$ are free of traction. Suppose, firstly, that a self-equilibrated load is applied to the arc $r = a$ and $b \to \infty$; intuitively one might expect the increasing area into which the stress is diffusing (that is, a geometric effect) to enhance the rate of decay of SVP when compared with the plate of constant thickness (that is the Papkovitch–Fadle solution, equivalent to $\alpha = 0$). However in one of the few works to consider explicitly the application of SVP to the wedge, Horvay (1957) employed an approximate variational approach, and concluded that the converse was true, at least for wedge angle $2\alpha \leqslant \pi$, and that attenuation was fastest when the edges of the wedge are parallel, "for there occurs more interference between the stresses, as they are reflected from the free edges, than in any other case".

This unexpected conclusion is here re-examined, and by expressing decay in terms of (*distance from the loaded arc*/*loaded arc length*), which conforms with the spirit of SVP, it is found that for all wedge angles the rate of decay is initially greater than for the strip, but as one moves away from the loaded edge so the rate of decay reduces; thus, if stress attenuation to 20% of the magnitude on $r = a$ is chosen as the criterion of rapidity, then decay is more rapid in the case of the wedge. On the other hand, if one chose stress attenuation to 2% then decay is more rapid in the case of parallel sides. (Of course one is attempting to compare exponential decay in the case of parallel sides with power law decay in the case of the wedge, so differences are to be expected; expressed in the above manner, the decay characteristics of the wedge and the plate are surprisingly similar.) One is led therefore to the conclusion that stress attenuation due to increased area (the geometric effect) is more important in the near-field close to the loaded arc, but of less importance in the far-field, when the free-edge effect of stress component interference becomes dominant.

Suppose, instead, that the self-equilibrated load is applied to the outer arc $r = b$; now the geometric effect of decreasing area would intuitively suggest an increase in stress (as is the case when the applied load constitutes a force or moment resultant), whereas the converging traction-free edges $\theta = \pm\alpha$ should be expected to enhance attenuation. If, as suggested above, the free edge effect is dominant over the geometric effect in the far-field, this would lead to the further unexpected result that decay to the 2% level is more rapid than for parallel sides; this is found to be the case for small wedge angles. However this argument must be qualified: for a self-equilibrated load on the arc $r = b$, one may only move radially a maximum distance b from the loaded arc; if the wedge

angle is small then this distance may be a sufficiently large multiple of the loaded arc length (which is $2\alpha b$) for the far-field effect to be dominant. On the other hand when wedge angle is large, then b may be only a small proportion of the loaded arc length, in which case there may not be a far-field, and the near-field geometric effect would then be dominant, and stress would increase as one moves away from the loaded arc. For example, when $\alpha = \pi/4$, the maximum radial span $b = 0.6366 \times (\textit{loaded arc length})$, and in the extreme case of $2\alpha = 2\pi$, then $(b/\textit{loaded arc length}) = 1/(2\pi) \approx 0.16$; in short, the geometry would not allow SVP to act.

Deliberating further, it seems reasonable to question how the two effects depend upon the wedge angle. The stresses σ_r and $\tau_{r\theta}$ on the generic arc, $r =$ constant, act over area $2r\alpha$ (per unit depth) while the self-equilibrated load is applied over area $2a\alpha$ (or $2b\alpha$); thus, the ratio of loaded area to the generic area varies in inverse proportion to the radius r, and one might suppose that the geometric effect is independent of the wedge angle 2α. Simultaneously the length of the traction-free edges, $(b-a)$, is independent of wedge angle, but as α increases so these traction-free edges must influence the stress on an increasing generic area $2r\alpha$, again suggesting that the free-edge effect will become of less importance as wedge angle increases.

Thus suppose, again, that the self-equilibrated load is applied on the arc $r = b$: for small wedge angles, attenuation due to free-edges should be greater than any stress increase due to area reduction, so stress levels would decrease as one moved away from the loaded arc, as is anticipated by SVP. As wedge angle increases, with the free-edge effect reducing in importance, then the constant geometric effect may become dominant and the self-equilibrated load would *not* decay but rather grow as one moves away from the loaded arc $r = b$. As will be seen this does indeed occur and the phenomenon of singular stress at a re-entrant corner may be attributed to this inapplicability of SVP: symmetric singular stress fields occur for $2\alpha > \pi$, whereas asymmetric singular fields occur for $2\alpha > 2\alpha^* \approx 1.43\pi$.

For the largest possible wedge angle, $2\alpha = 2\pi$, the problem becomes that of the stress field in the vicinity of a crack tip, which is the discipline of LEFM, first treated by Williams (1957) using the Airy stress function approach also employed here; in LEFM the plane symmetric and asymmetric stress distributions, which are the same for all crack tips—only the magnitudes, the well known stress intensity factors, depend on the geometry of the structure and the magnitude of the applied load— are described as Mode I (opening) and Mode II (sliding), respectively. It will be seen that these unique crack tip distributions may be attributed to SVP inapplicability for just one particular eigenmode (corresponding to one particular stress distribution). A similar situation occurs for Mode III (tearing), this simpler anti-plane problem having been considered by Stephen and Wang (1996).

For completeness, a brief theoretical treatment is provided; the major contribution in the present work is a re-examination and interpretation of the predictions of that theory.

2. Theory

2.1. *General solution*

Consider the plane strain isotropic elastic wedge occupying the region

$$a \leqslant r \leqslant b, \quad -\alpha \leqslant \theta \leqslant +\alpha, \quad -\infty < z < \infty, \tag{1}$$

where r, θ and z are cylindrical coordinates; body forces are assumed absent and the flanks of the wedge, $\theta = \pm\alpha$, are free of traction. The Airy stress function must satisfy the biharmonic equation

$$\nabla^4\phi = 0, \tag{2}$$

and is taken in the form

$$\phi = (r/r_0)^{-\lambda} f(\theta) = (r/r_0)^{-\lambda}\exp(ik\theta), \tag{3}$$

where $i = (-1)^{1/2}$, and r_0 is an arbitrary constant having dimension length; eqn (2) leads to the characteristic equation

$$[k^4 - k^2(\lambda^2 + (\lambda+2)^2) + \lambda^2(\lambda+2)^2] = 0, \tag{4}$$

which has solutions

$$k = \pm\lambda, \quad \pm(\lambda+2). \tag{5}$$

The stress function then becomes

$$\phi = (r/r_0)^{-\lambda}\,[C_1\cos\lambda\theta + C_2\sin\lambda\theta + C_3\cos(\lambda+2)\theta + C_4\sin(\lambda+2)\theta], \tag{6}$$

where $C_{1,2,3,4}$ are constants. Accordingly the stress components are

$$\begin{aligned}
\sigma_r &= \partial\phi/r\,\partial r + \partial^2\phi/r^2\,\partial\theta^2 \\
&= -(r/r_0)^{-\lambda-2}(\lambda+1)[C_1\lambda\cos\lambda\theta + C_2\lambda\sin\lambda\theta + C_3(\lambda+4)\cos(\lambda+2)\theta \\
&\quad + C_4(\lambda+4)\sin(\lambda+2)\theta]/r_0^2, \\
\sigma_\theta &= \partial^2\phi/\partial r^2 \\
&= (r/r_0)^{-\lambda-2}(\lambda+1)[C_1\lambda\cos\lambda\theta + C_2\lambda\sin\lambda\theta + C_3\lambda\cos(\lambda+2)\theta + C_4\lambda\sin(\lambda+2)\theta]/r_0^2, \\
\tau_{r\theta} &= -(\partial/\partial r)(\partial\phi/r\,\partial\theta) \\
&= (r/r_0)^{-\lambda-2}(\lambda+1)[-C_1\lambda\sin\lambda\theta + C_2\lambda\cos\lambda\theta - C_3(\lambda+2)\sin(\lambda+2)\theta \\
&\quad + C_4(\lambda+2)\cos(\lambda+2)\theta]/r_0^2.
\end{aligned} \tag{7}$$

The displacement components are obtained from the strains by integration as

$$\begin{aligned}
u_r &= (1+v)(r/r_0)^{-\lambda-1}[C_1\lambda\cos\lambda\theta + C_2\lambda\sin\lambda\theta + C_3(v+\lambda)\cos(\lambda+2)\theta \\
&\quad + C_4(v+\lambda)\sin(\lambda+2)\theta]/Er_0, \\
u_\theta &= (1+v)(r/r_0)^{-\lambda-1}\,[C_1\lambda\sin\lambda\theta - C_2\lambda\cos\lambda\theta + C_3(\lambda+2-v)\sin(\lambda+2)\theta
\end{aligned}$$

$$-C_4(\lambda+2-v)\cos(\lambda+2)\theta]/Er_0, \tag{8}$$

where $v = 4/(1+v)$, v is Poisson's ratio, and E is Young's modulus.

2.2. *Symmetric loading*

Consider first the symmetric case and impose boundary conditions

$$\sigma_\theta = \tau_{r\theta} = 0 \quad \text{on } \theta = \alpha, \quad \text{and} \quad u_\theta = 0 \quad \text{on } \theta = 0. \tag{9}$$

The constants C_2 and C_4 are zero and this leads to the eigenequation

$$(\lambda+1)\sin 2\alpha + \sin 2(\lambda+1)\alpha = 0. \tag{10}$$

The stresses and displacements may then be obtained by writing

$$C_1 = -C_3 \frac{(\lambda+2)\sin(\lambda+2)\alpha}{\lambda \sin \lambda\alpha} \tag{11}$$

in eqns (7) and (8).

2.3. *Asymmetric loading*

For the asymmetric case

$$u_\theta(\theta) = u_\theta(-\theta), \quad \text{or } u_r = 0 \quad \text{on } \theta = 0, \tag{12}$$

from which constants C_1 and C_3 are zero, and the traction-free condition

$$\sigma_\theta = \tau_{r\theta} = 0 \quad \text{on } \theta = \alpha, \tag{13}$$

leads to the eigenequation

$$(\lambda+1)\sin 2\alpha - \sin 2(\lambda+1)\alpha = 0. \tag{14}$$

The stresses and displacements may then be obtained by writing

$$C_2 = -C_4 \frac{\sin(\lambda+2)\alpha}{\sin \lambda\alpha} \tag{15}$$

in eqns (7) and (8).

Note that the asymmetric eigenequation (14) is satisfied for all wedge angles by the eigenvalue $\lambda = -2$; the stresses are zero and the displacement components indicate a (asymmetric) rigid body rotation only about the origin. However, as will be seen in Section 4, there are further solutions

valid only at the critical semi-wedge angle $\alpha = \alpha^*$, for the asymmetric case, and valid only at angles $\alpha = \pi/2$ and π, for the symmetric case; in both cases, the stress fields are self-equilibrating and are independent of radius, indicating SVP inapplicability.

Both eigenequations (10) and (14) are satisfied for all wedge angles by the eigenvalue $\lambda = -1$; the stresses are again zero, and the displacement components reduce to $u_r = 4C_3 \cos\theta/Er_0$, $u_\theta = -4C_3 \sin\theta/Er_0$, which is a (symmetric) rigid body displacement in the x-direction, and $u_r = 4C_4 \sin\theta/Er_0$, $u_\theta = 4C_4 \cos\theta/Er_0$, which is a (asymmetric) rigid body displacement in the y-direction. As will be seen in Section 3, the root $\lambda = -1$ is also associated with a simple radial stress distribution.

3. Radial variation in stress

3.1. *Diffusion of stress resultants*

Firstly some well known (see Massonnet, 1962) stress distributions for the wedge are noted, for which the applied load constitutes a stress resultant; radial variation in stress level is then purely a geometric effect of diffusion of stress into a divergent or convergent area.

3.1.1. *Diffusion of force*

Both eigenequations (10) and (14) are satisfied by $\lambda = -1$ for all wedge angles; besides the rigid body translations already noted, from eqn (5) the roots are

$$k = \mp 1, \quad \pm 1, \tag{16}$$

and the multiplicity indicates that the stress function should take the form

$$\phi = (r/r_0)\,[(C_1 + C_2\theta)\sin\theta + (C_3 + C_4\theta)\cos\theta], \tag{17}$$

where $C_{1,2,3,4}$ are constants. This is the Flamant solution and gives rise to a distribution of purely radial stress, both symmetric ($C_4 = 0$) and asymmetric ($C_2 = 0$),

$$\begin{aligned} \sigma_r &= 2(C_2 \cos\theta - C_4 \sin\theta)/r_0 r, \\ \sigma_\theta &= 0, \\ \tau_{r\theta} &= 0. \end{aligned} \tag{18}$$

This distribution on an arc of constant radius may constitute a force resultant per unit depth[1] in the x-direction (the symmetric case) given by

[1] The force resultants are $R_x = -r\int_{-\alpha}^{\alpha}(\sigma_r \cos\theta - \tau_{r\theta}\sin\theta)\,\mathrm{d}\theta$, $R_y = -r\int_{-\alpha}^{\alpha}(\sigma_r \sin\theta + \tau_{r\theta}\cos\theta)\,\mathrm{d}\theta$.

$$R_x = -C_2(2\alpha+\sin 2\alpha)/r_0$$

and a shearing force in the y-direction (the asymmetric case)

$$R_y = C_4(2\alpha-\sin 2\alpha)/r_0,$$

together with a bending moment

$$M = rR_y.$$

Thus, for a compressive force R_x in the x-direction the radial stress is

$$\sigma_r = -2R_x\cos\theta/(r(2\alpha+\sin 2\alpha)) \tag{19}$$

which agrees with the intuitive expectation that since stress is force/area, and the area carrying the load increases linearly with radius, so stress should vary inversely with the radius. Similarly the bending moment produced by a force R_y in the y-direction gives the radial stress

$$\sigma_r = -2R_y\sin\theta/(r(2\alpha-\sin 2\alpha)); \tag{20}$$

this variation is consistent with the expectation that for a beam of linearly varying depth, where the second moment of area varies as r^3, and the bending moment varies linearly with r, so the bending stress along a fibre defined by θ = constant (whose distance from the neutral axis varies linearly with r) should be inversely proportional to radius.

3.1.2. *Diffusion of concentrated moment*

The asymmetric eigenequation (14) is satisfied by $\lambda = 0$ for all α, which is a double root; the stress function should then have the form

$$\phi = C_1 + C_2\theta + C_3\cos 2\theta + C_4\sin 2\theta. \tag{21}$$

The stresses are

$$\begin{aligned}\sigma_r &= -4(C_3\cos 2\theta + C_4\sin 2\theta)/r^2,\\ \sigma_\theta &= 0\\ \tau_{r\theta} &= (C_2 - 2C_3\sin 2\theta + 2C_4\cos 2\theta)/r^2.\end{aligned} \tag{22}$$

The constant C_3 is immediately zero from the requirement of asymmetry (this is also the condition that resultant R_x should be zero), while the relationship $C_2 = -2C_4\cos 2\alpha$ arises from the traction-free condition $\tau_{r\theta} = 0$ on $\theta = \pm\alpha$ (this is also the condition that resultant R_y should be zero). The distribution becomes

$$\sigma_r = -4C_4\sin 2\theta/r^2,$$

$$\sigma_\theta = 0,$$
$$\tau_{r\theta} = 2C_4(\cos 2\theta - \cos 2\alpha)/r^2. \tag{23}$$

The constant C_4 is evaluated by requiring that the moment about the origin $r = 0$ (i.e. $M = r^2 \int_{-\alpha}^{\alpha} \tau_{r\theta}\, d\theta$) should be equal to the applied moment M, which gives

$$M = 2C_4(\sin 2\alpha - 2\alpha \cos 2\alpha). \tag{24}$$

The stresses are then

$$\sigma_r = -2M \sin 2\theta/(r^2(\sin 2\alpha - 2\alpha \cos 2\alpha))$$
$$\sigma_\theta = 0,$$
$$\tau_{r\theta} = M(\cos 2\theta - \cos 2\alpha)/(r^2(\sin 2\alpha - 2\alpha \cos 2\alpha)), \tag{25}$$

which is known in the literature as the Carothers solution; the radial variation is consistent with the expectation that bending stress along a fibre $\theta =$ constant, for a beam of linearly varying depth, should vary as r^{-2} for pure bending. A discussion of the breakdown of this solution at the critical wedge angle $2\alpha^* \approx 1.43\pi$, attempts at its repair, and the relationship with SVP, is given in Section 4.

3.2. *Decay of self-equilibrated loading*

Now consider the locus of roots of the symmetric eigenequation (10), the real parts of which are shown in Fig. 1. Firstly one notes that the branches are symmetric about $\lambda = -1$; thus for $\alpha = \pi/6$, the smallest (complex) roots are $\lambda = 3.0593 \pm 1.9520i$ and the corresponding mirror image branch has $\lambda = -5.0593 \pm 1.9520i$. Secondly, it is noted that stress varies with radius as $(r/r_0)^{-\lambda-2}$; thus, the root $\lambda = -2$ corresponds to a stress distribution independent of radius. For roots in which the real part $\mathbb{R}(\lambda) > -2$, stresses decrease as radius increases, and this corresponds to decay of a self-equilibrated loading on the inner arc $r = a$. Similarly for roots having $\mathbb{R}(\lambda) < -2$, stresses decrease as radius decreases which, in the main, corresponds to decay of a self-equilibrated loading on the outer arc $r = b$.

3.2.1. *Decay from inner arc $r = a$*

Consider the decay of stress away from a self-equilibrated load on the inner arc $r = a$, and in particular the minimum rate of decay which validates SVP and indicates the maximum depth of penetration of the stress. In order to judge the effect of the divergent area, and also to re-examine the Horvay (1957) conclusion, the present results are compared with stress decay for the plane strain semi-infinite plate, the well known Papkovitch–Fadle solution (see Timoshenko and Goodier (1970), article 26) where, for the symmetric case, the minimum rate of decay is $\exp(-2.1061z/c) = \exp(-4.2122z/t)$; here $t = 2c$ is the plate thickness over which the self-equilibrated load is applied, and z is distance from the loaded edge. To facilitate comparison, the wedge power law decay must be expressed in a similar vein; thus, noting that distance from the loaded

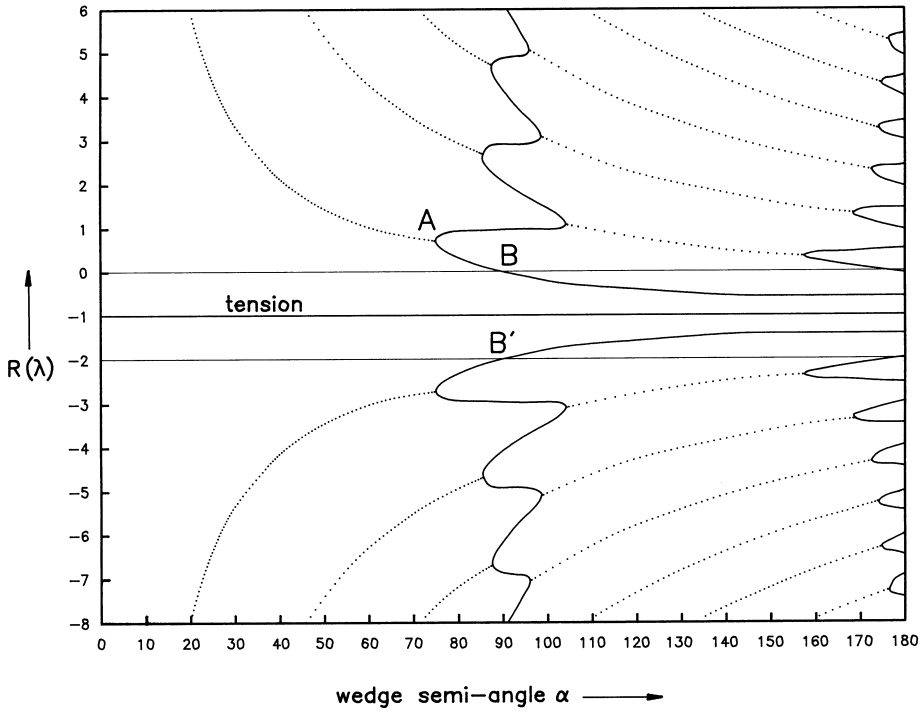

Fig. 1. Locus of roots: symmetric case. Solid and dotted lines represent real and complex roots respectively. The lines $\lambda = 0$ and $\lambda = -2$ are not roots, but have been inserted as a grid reference.

arc, $(r-a)$, takes the place of z, and that plate thickness t is effectively replaced by inner arc length $(s = 2a\alpha)$, then the power law variation of stress level with radius, i.e. $(r/r_0)^{-\lambda-2}$ may be expressed as

$$\left(1+2\alpha\left(\frac{\textit{distance from loaded arc}}{\textit{arc length}}\right)\right)^{-\lambda-2},$$

where the arbitrary constant r_0 has been set equal to the inner arc radius a.The decay characteristics are shown in Fig. 3, together with the diffusion of the symmetric stress resultant, that is a tension, and it is seen that for any given wedge angle the self-equilibrated load decays more rapidly than does a tensile force due to diffusion into the divergent area, as should be the case according to conventional interpretation of SVP; by expressing stress variation in this way, the decay characteristics for all wedge angles fall into a fairly tight band. For all wedge angles, the rate of decay is initially more rapid than for the plate, suggesting that the geometric effect is more important in the near-field. However as one moves away from the loaded arc, so the decay rate becomes less than the exponential decay of the plate, as presaged in the Introduction. These differences in the decay characteristics of self-equilibrated loading, and in particular the fact that divergent area enhances decay in the near field, when compared with the exponential decay characteristic, can be

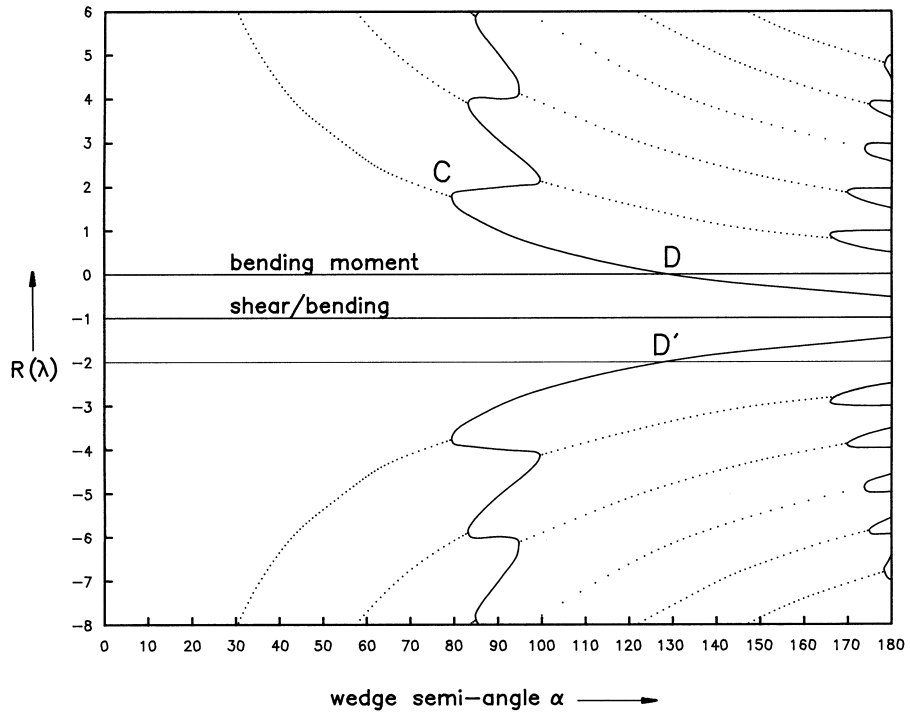

Fig. 2. Locus of roots: asymmetric case. Solid and dotted lines represent real and complex roots respectively. The line $\lambda = -2$ is not a root, but has been inserted as a grid reference.

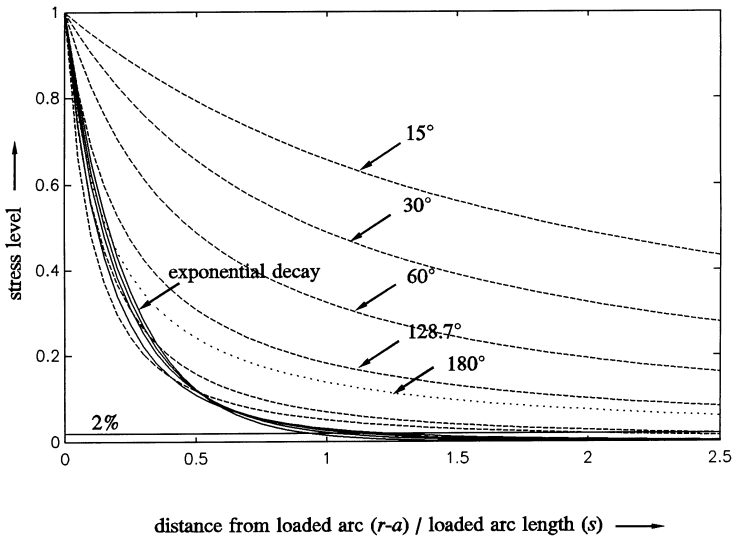

Fig. 3. Decay of symmetric load, both self-equilibrating and tension, from the inner arc $r = a$. Tensile forces are annotated according to the wedge semi-angle α.

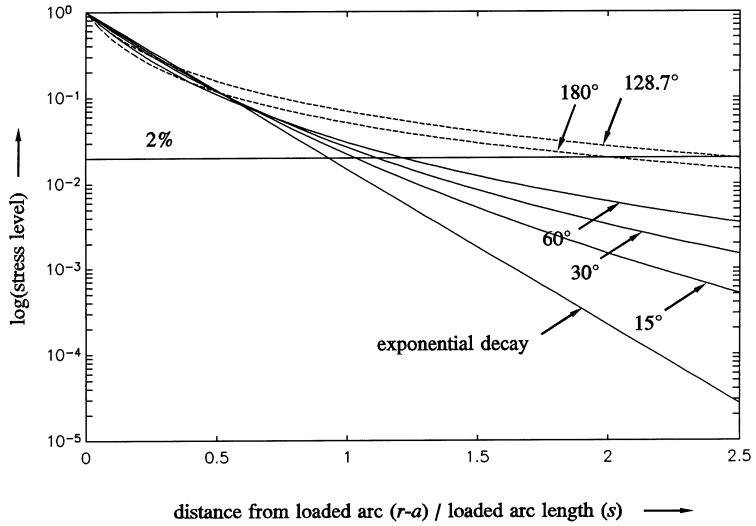

Fig. 4. Decay of self-equilibrated symmetric load from inner arc $r = a$.

seen more clearly in Fig. 4 where log(stress) is shown together with the 2% level, which in the study of dynamics is taken as the duration of an exponential decay, $\exp(-t/\tau)$. (This is normally taken as four time constants, 4τ, when stress level has reduced to 1.8%.) Surprisingly, the minimum decay rate in the far field occurs for the critical angle α^* rather than for $\alpha = \pi$.

Differences in decay characteristic, over the range of possible wedge angle, can also be seen in Fig. 5, which shows the maximum depth of penetration of the self-equilibrated load, that is the number of arc lengths one must move away from the loaded arc for stress to decay to the 2% level. (For parallel sides, $z = 0.9287t$ for the symmetric case; that is, stress will decay to 2% of edge value at a distance of $0.9287 \times$ plate thickness.) It is seen that the depth of penetration increases for all non-zero α, although the wedge angle must become large before the increase is significant. Thus, at $\alpha = \pi/3$ the penetration depth increases by approximately 30% over the plate value. For the symmetric case, the curve shows a discontinuity at point A, $\alpha \approx 73^\circ$, when the previously complex smallest root becomes real at the bifurcation point A on Fig. 1. For $\alpha > 73^\circ$ the smallest root in Fig. 1 initially reduces rapidly, resulting in less rapid stress decay and increasing depth of penetration of the self-equilibrated edge load. Returning to Fig. 5 it is seen that the maximum depth of penetration (at just under $2.5 \times$ arc length) occurs for the critical wedge angle α^*. As α is increased beyond this critical angle, the maximum penetration depth then decreases to a value $2.0009 \times$ arc length for $\alpha = \pi$. Also shown in Fig. 5 is the depth of penetration (using the same 2% criterion) of a bending moment, and it is seen that conventional interpretation of SVP applicability extends only to the half-space, $\alpha = \pi/2$, when the "slowest" symmetric self-equilibrated load penetrates to the same depth as does the (asymmetric) bending moment, at point B.

Next consider the asymmetric case: the locus of roots, Fig. 2, is again symmetrical about $\lambda = -1$; thus, for a wedge having $\alpha = \pi/3$ the smallest (complex) root is $\lambda = 2.6307 \pm 0.8812i$, and the mirror image branch has $\lambda = -4.6307 \pm 0.8812i$. Again the rate of stress decay away from the

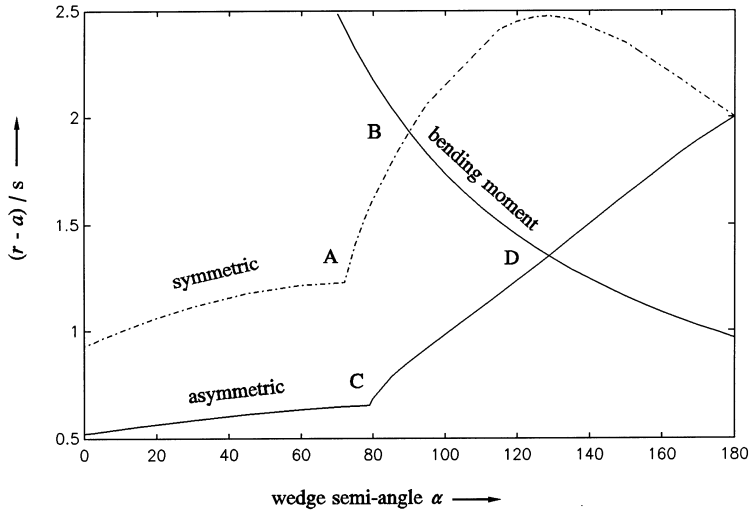

Fig. 5. Stress penetration from inner arc $r = a$: number of arc lengths ($s = 2\alpha a$) to decay to 2%.

loaded arc is compared with the Papkovitch–Fadle solution for the plate, which has slowest decay as $\exp(-3.7488z/c) = \exp(-7.4976z/t)$. Again the depth of stress penetration, Fig. 5, increases for all α, and the wedge angle 2α must become large before the increase is significant. Now there is a discontinuity at point C, $\alpha \approx 79^\circ$, where the smallest complex root becomes real at the bifurcation point C on Fig. 2. The penetration depth then increases almost linearly with α to the value 2.0009 × arc length for $\alpha = \pi$, which is identical to the penetration depth for the symmetric case, both cases having smallest root $\lambda = -1/2$ at $\alpha = \pi$. Now it is seen that the depth of penetration of the "slowest" asymmetric self-equilibrated stress is the same as that of the bending moment at point D, Figs 2 and 5, the critical wedge angle $2\alpha^*$, again indicating SVP inapplicability according to conventional interpretation. The actual decay of stress is shown in Fig. 6, together with the diffusion of the concentrated moment; as with the symmetric case, the geometric effect of divergent area leads to a more rapid decay in the near-field, close to the loaded arc, when compared with the exponential decay characteristic of the plate; in contrast with the symmetric case, the decay of a moment due to diffusion into the diverging area can be more rapid than the decay of a self-equilibrating load. Thus in Fig. 6, the line annotated as 128.7° is both Saint-Venant decay and diffusion of the moment, and for the case $\alpha = \pi$ the self-equilibrated load (annotated from below) decays less rapidly than the moment (annotated from above) diffuses. The band of decay characteristics of the self-equilibrated load is now not so tight as for the symmetric case.

Thus far, discussion has concentrated on the decay of stress away from a self-equilibrated load on the arc $r = a$, associated with the positive (real) roots λ in Figs 1 and 2. Intuitively one expects such decay by virtue of two agencies: the first is the increased area which carries the self-equilibrated load as one moves away from the arc $r = a$, as seen previously for those stress distributions which do constitute a force or moment resultant, Section 3.1. The second agent is the traction-free edge effect, and for a self-equilibrated load on the arc $r = a$ both these effects work in concert to give

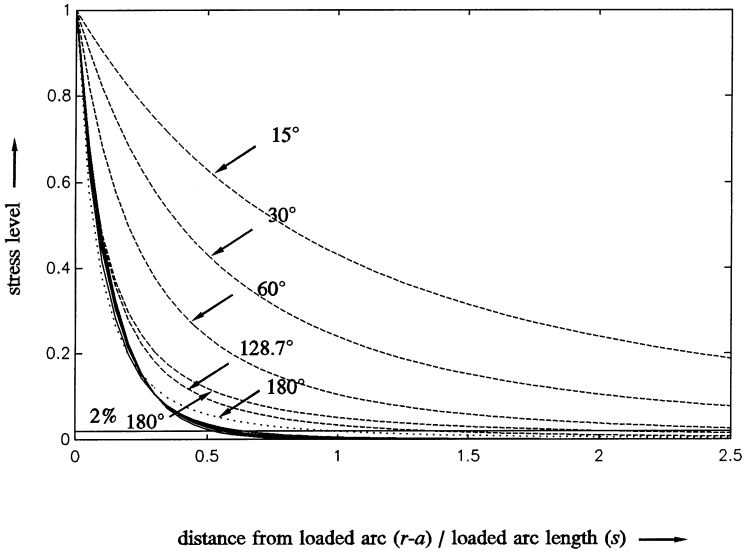

Fig. 6. Decay of asymmetric load, both self-equilibrating and concentrated moment, from inner arc $r = a$. Moments are annotated from above according to the wedge semi-angle α.

the overall decay characteristic; the manifestation of SVP inapplicability is that a self-equilibrated load can decay at the same rate as a bending moment diffuses into a divergent area.

3.2.2. *Decay from the outer arc $r = b$*

Suppose, instead, that the self-equilibrated load is applied on the arc $r = b$: the two effects no longer work together, but rather in opposition. Thus, as one moves away from the loaded arc (that is, as radius decreases) so the geometric effect of reduced area should be expected to give an increase in stress level (this is the case for distributions constituting a resultant, Section 3.1), whereas SVP (the free-edge effect) would suggest that stress levels should decrease. Since these two effects act in opposition one should expect less rapid decay away from the loaded arc in the case of a self-equilibrated load; thus, consider the symmetric case, $\alpha = \pi/6$, when the smallest root for a self-equilibrated load on $r = a$ has $\mathbb{R}(\lambda) = 3.0593$ and stress varies with radius as $r^{-\lambda-2} = r^{-5.0593}$. For a load on $r = b$, the image root of Fig. 1 has $\mathbb{R}(\lambda) = -5.0593$ when stress varies as $r^{-\lambda-2} = r^{3.0593}$. Thus, the theoretical predictions agree with one's intuitions: stresses due to a self-equilibrated load decay as one moves away from the loaded arc $r = b$, as SVP says they should, but the decay is less rapid due to the geometric effect of reducing area.

Turning to Fig. 7, it is seen that for the small wedge angles shown, $\alpha \leqslant 15^\circ$, decay to 2% is more rapid than for the case of parallel sides, as one would expect from an enhanced far-field free-edge effect, although in the near-field decay is less rapid than exponential, as one would expect from the convergent area. However, as wedge angle increases one would expect the far-field dominance to become less important: thus, for a wedge angle $\alpha = \pi/6$, say, it is only possible to move a maximum radial distance of $0.955 \times$ (loaded arc length) from the loaded arc, and it is natural to ask whether the near-field increase in stress level due to convergent area is ever sufficiently large to overcome the far-field stress reduction if, indeed, there is a far-field. Again note that stress is

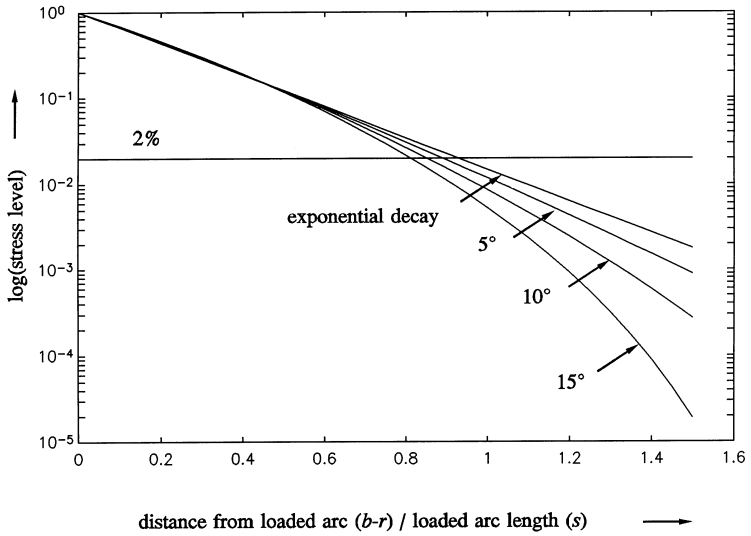

Fig. 7. Decay of self-equilibrated symmetric load from outer arc $r = b$, for small semi-wedge angles α.

independent of radius if $\mathbb{R}(\lambda) = -2$; if $\mathbb{R}(\lambda) < -2$ then stress level will decay as one moves away from the arc $r = b$, and SVP is applicable, although the rate of decay may not be rapid. This is true for all of the mirror image root loci except for the "slowest" decay branch which has $\mathbb{R}(\lambda) \geqslant -2$ for $\alpha \geqslant \pi/2$ for the symmetric case, Fig. 1, and $\mathbb{R}(\lambda) \geqslant -2$ for $\alpha \geqslant \alpha^*$ for the asymmetric case, Fig. 2. For these portions of just two decay branches, the geometric effect is dominant; thus, stress levels are increasing due to convergent area more rapidly than they are decreasing by virtue of the free-edge effect, indicating the anticipated inapplicability of SVP.

In the case of $\alpha = \pi$, which is the idealised unloaded crack of LEFM, both the symmetric and asymmetric cases have $\lambda = -3/2$, which corresponds to the familiar stress field in the vicinity of the crack tip, when the constants C_3 and C_4 are related to the stress intensity factors K_1 and K_{11}, respectively.[2] Suppose an arbitrary self-equilibrated load is applied to the outer arc; since this load is periodic in θ, it may be expanded as the summation of stress terms as in eqn (7) with $\lambda = -3/2$, -2, $-5/2$, -3, etc. For all these terms, with the exception of $\lambda = -3/2$, the decay of SVP is dominant over the geometric effect, and such stresses would not reach the crack tip. Thus, whatever the distribution on $r = b$, the crack tip distribution has $\lambda = -3/2$, and the unique Mode I and Mode II stress distributions in the vicinity of the crack tip, which is at the heart of LEFM, may be attributed to SVP inapplicability for just one eigenmode for each of the symmetric and asymmetric cases; the only remaining question is the intensity of the applied stress distribution on the arc $r = b$, which in turn defines the stress intensity factor of LEFM.

4. The wedge paradox

At first sight eqns (25) suggest that the stresses become everywhere infinite for the wedge semi-angle α^* which satisfies

[2] The relationships are $K_1 = C_3(2\pi)^{1/2} r_0^{-3/2}$, $K_{11} = -C_4(2\pi)^{1/2} r_0^{-3/2}$.

$$\sin 2\alpha^* - 2\alpha^* \cos 2\alpha^* = 0, \quad \alpha^* \approx 0.715\pi \approx 128.7^\circ. \tag{26}$$

This "pathological" behaviour of the Carothers solution has been considered by numerous authors, and many have concurred with the view that the stresses σ_r and $\tau_{r\theta}$ theoretically become infinitely large when $\alpha = \alpha^*$; more circumspect analysis has shown that the stresses according to eqns (25) are merely undefined as, from eqn (24), it is clear that at this particular wedge angle the bending moment M is zero, and loading on the arc $r = a$ is self-equilibrating. Sternberg and Koiter (1959), and later Markenscoff (1994), recognised this as a breach of SVP applicability since, for angles greater than the critical angle, a self-equilibrated loading on the arc $r = a$ can decay less rapidly than the decay (or, more precisely, the diffusion into a diverging area) of a bending moment.

Various authors (Neuber, 1963; Dempsey, 1981; Ting, 1984, 1985; Leguillon, 1988) have attempted to repair the Carothers solution at, and close to, the critical wedge angle by the introduction of a logarithmic stress singularity; while the resulting stress field may constitute a moment at the critical angle, it has been remarked by Markenscoff (1994) that it is "deficient in the sense that it gives infinite moment resultant on arcs of arbitrary length at infinity. Only on the total wedge angle the resultant moment is M (being the finite difference of two infinities)."

However, what these authors have not considered is the wider inapplicability of SVP, in relation to loading on the outer arc $r = b$, in particular the case of $\lambda = -2$. The asymmetric eigenequation (14) is satisfied identically, while eqns (7) and (8) reveal nothing other than the rigid body displacements; however, the characteristic eqn (4) has roots $k = \pm 0, \pm 2$, which are identical to those for the concentrated moment problem, Section 3.1.2, in which case the resulting stress function

$$\phi = (r/r_0)^2 [C_1 + C_2\theta + C_3 \cos 2\theta + C_4 \sin 2\theta], \tag{27}$$

has identical θ-dependence [cf eqn (21)]. The traction-free condition $\tau_{r\theta} = 0$ on $\theta = \pm\alpha$ leads to $C_3 = 0$, and $C_2 = -2C_4 \cos 2\alpha$, while the condition $\sigma_\theta = 0$ on $\theta = \pm\alpha$ leads to $C_1 = 0$, and $C_2\alpha = -C_4 \sin 2\alpha$. These relationships between C_2 and C_4 require either $C_2 = C_4 = 0$, or $2\alpha \cos 2\alpha - \sin 2\alpha = 0$, which is satisfied by $\alpha = \alpha^*$. Thus, the root $\lambda = -2$ leads to the self-equilibrated stress distribution

$$\begin{aligned} \sigma_r &= -2C_4(2\theta \cos 2\alpha^* + \sin 2\theta)/r_0^2, \\ \sigma_\theta &= -2C_4(2\theta \cos 2\alpha^* - \sin 2\theta)/r_0^2, \\ \tau_{r\theta} &= -2C_4(\cos 2\theta - \cos 2\alpha^*)/r_0^2, \end{aligned} \tag{28}$$

which is valid only for the critical angle, α^*; since the components are independent of the radial coordinate r, one has an asymmetric self-equilibrated load which can be present on both inner and outer arcs, and which does not decay in either radial direction, marking the inapplicability of SVP. This field has previously been derived by Ting (1984), but its significance in relation to SVP was not noted.

For the symmetric case, Fig. 1, the root $\lambda = -2$ is valid only at $\alpha = \pi/2$ and π, and gives the stress field

$$\sigma_r = -2C_3(\pm\cos 2\theta - 1)/r_0^2,$$
$$\sigma_\theta = 2C_3(1 \pm \cos 2\theta)/r_0^2,$$
$$\tau_{r\theta} = \pm 2C_3 \sin 2\theta/r_0^2, \tag{29}$$

where the positive and negative signs pertain to $\alpha = \pi/2$ and π, respectively. In the case of the half-space, $\alpha = \pi/2$, one again has a self-equilibrating stress field which is independent of radius. For the crack problem, $\alpha = \pi$, these components are often overlooked for the symmetric case, or incorrectly assumed to be present in the asymmetric case, and are of relevance in the collocation method for determination of the stress intensity factor.

5. Conclusions

The decay of self-equilibrated loading applied to the inner or outer arc of a plane strain elastic wedge has been considered in terms of a near-field geometric effect, and a far-field stress interference effect at a traction-free edge. For loading on the inner arc, the two effects act in concert; however for loading on the outer arc the two effects act in opposition, with the far-field effect becoming less influential as wedge angle increases. Saint-Venant's principle becomes inapplicable for a wedge angle in excess of the half-space, when

(a) symmetric self-equilibrated loading on the inner arc can decay less rapidly than does a bending moment, the latter due to stress diffusion into a divergent area.
(b) symmetric self-equilibrated loading on the outer arc can increase as one moves away from the loaded arc, the geometric effect being dominant.

For the wedge angle $2\alpha = 2\pi$ the unique Modes I and II inverse square root stress singularities at the crack tip, which are at the heart of LEFM, can be attributed to an inapplicability of Saint-Venant's principle for just one symmetric and one asymmetric eigenmode.

References

Carothers, S.D., 1912. Plane strain in a wedge. Proceeding of the Royal Society of Edinburgh 23, 292–306.
Dempsey, J.P., 1981. The wedge subjected to tractions: a paradox resolved. Journal of Elasticity 11, 1–10.
Dundurs, J., Markenscoff, X., 1989. The Sternberg–Koiter conclusion and other anomalies of the concentrated couple. Transactions ASME Journal of Applied Mechanics 56, 240–245.
Horvay, G., 1957. Saint-Venant's principle: a biharmonic eigenvalue problem. Transactions of ASME Journal of Applied Mechanics 24, 381–386.
Leguillon, D., 1988. Sur le moment ponctuel appliqué à un secteur: le paradoxe de Sternberg–Koiter. C.R. Acad. Sci. Paris, series II, 307, 1741–1746.
Markenscoff, X., 1994. Some remarks on the wedge paradox and Saint-Venant's principle. Transactions ASME Journal of Applied Mechanics **61,** 519–523.
Massonnet, C., 1962. Two-dimensional problems. In Handbook of Engineering Mechanics, chap. 37, ed. W. Flugge. McGraw-Hill.
Neuber, H., 1963. Lösung des Carothers-Problems mittels Prinzipien der Kraftübertragung (Keil mit Moment an der Spitze). Zeitschrift fur Angewandte Mathematik und Mechanik 43, 211–228.

Stephen, N.G., Wang, P.J., 1966. Saint-Venant's principle and the anti-plane wedge. I. Mech. E. Journal of Strain Analysis for Engineering Design 31, 231–234.

Sternberg, E., Koiter, W. T., 1958. The wedge under a concentrated couple: a paradox in the two-dimensional theory of elasticity. Transactions ASME Journal of Applied Mechanics 25, 575–581. See also the discussion on this by various authors in (1959) in Transactions ASME Journal of Applied Mechanics 26, 472–474.

Timoshenko, S.P., Goodier, J.N., 1970. Theory of Elasticity, 3rd edn. McGraw-Hill.

Ting, T.C.T., 1984. The wedge subjected to tractions: a paradox re-examined. Journal of Elasticity 14, 235–247.

Ting, T.C.T., 1985. A paradox on the elastic wedge subjected to a concentrated couple and on the Jeffery–Hamel viscous flow problem. Zeitschrift fur Angewandte Mathematik und Mechanik 65, 188–190.

Williams, M., 1957. On the stress distribution at the base of a stationary crack. Transactions ASME Journal of Applied Mechanics 24, 109–114.